Diffuse Charge Effects in Fuel Cell Membranes

P. Maarten Biesheuvel,[a,b,z] **Alejandro A. Franco,**[c,*] **and Martin Z. Bazant**[d,e,*]

[a]*Department of Environmental Technology, Wageningen University, Wageningen,
The Netherlands*
[b]*Materials Innovation Institute, Delft, The Netherlands*
[c]*Commissariat à l'Energie Atomique/DRT/LITEN/Département des Technologies de l'Hydrogène/
Laboratoire de Composants PEM, 38000 Grenoble, France*
[d]*Departments of Chemical Engineering and Mathematics, Massachusetts Institute of Technology,
Cambridge, Massachusetts 02139, USA*
[e]*UMR Gulliver 7083, ESPCI-CNRS, 75005 Paris, France*

It is commonly assumed that electrolyte membranes in fuel cells are electrically neutral, except in unsteady situations, when the double-layer capacitance is heuristically included in equivalent circuit calculations. Indeed, the standard model for electron transfer kinetics at the membrane/electrode interface is the Butler–Volmer equation, where the interfacial overpotential is based on the total potential difference between the electrode and bulk electrolyte. Here, we develop an analytical theory for a solid-state proton-conducting membrane that accounts for diffuse charge in the electrostatic polarization layers and illustrate its use for a steady-state hydrogen concentration cell. The theory predicts that the total membrane charge is nonzero, except at a certain hydrogen pressure, which is a thermodynamic constant of the fuel cell membrane. Diffuse layer polarization introduces the Frumkin correction for reaction rates, where the overpotential is based on the potential difference across only the compact (Stern) part of the polarization layer. In the Helmholtz limit of a relatively thin diffuse layer, we recover well-known results for a neutral membrane; otherwise, we predict significant effects of diffuse charge on the electron-transfer rate. Our analysis also takes into account the excluded volume of solvated protons, moving in a uniform charge density of fixed anions.
© 2008 The Electrochemical Society.   [DOI: 10.1149/1.3021035] All rights reserved.

One of the key elements in electrochemical processes is the transfer of electrical charge across the electrode-electrolyte interface. The kinetics of this reaction is commonly described by the Butler–Volmer (BV) equation, which is formulated as the difference between an anodic and a cathodic reaction rate. These reaction rates depend on the concentrations of the participating atoms and ions and on the interfacial overpotential, which describes the influence of the step in potential of the electron when going from the electrode into the electrolyte phase and vice versa.[1-5] The overpotential is typically defined as the potential drop across the entire double layer, between the electrode and the neutral bulk electrolyte, relative to the equilibrium state, where the net Faradaic current is zero. As emphasized long ago by Frumkin,[6] it is more accurate to evaluate the concentrations where the reaction actually occurs, at the hypothetical "outer Helmholtz plane" or "pre-electrode plane," which is the distance of closest approach to the electrode for a solvated ion, separated from the electrolyte bulk by the polarization layer ("diffuse layer" or "space-charge region"); see Fig. 1a.[2,7-10] This introduces the so-called Frumkin correction to the BV equation, where the overpotential is based on the potential step from metal to the reaction plane, across only the charge-free compact layer (the "Stern layer," "compact layer," or "inner layer"), and not including the diffuse layer. In describing reaction rates, the compact layer is commonly described as a flat, uncharged, uniform dielectric film on the electrode. With this approach, the Frumkin correction has been included in a few general models of thin electrochemical cells, for example, by Itskovich et al.[11] and Kornyshev and Vorotyntsev,[12,13] who also included ion volume constraints for a solid electrolyte with a single mobile ion, and by Bonnefont et al.,[9] Bazant et al.,[14] and Chu and Bazant.[15]

In models of fuel cells, diffuse charge is almost always neglected and the ion-conducting membrane is assumed to be electrically neutral. Indeed, for fuel cell modeling including diffuse charge, we are only aware of the work by Franco et al.,[10,16] where Frumkin-corrected electron transfer equations are used, within the framework of transition state theory, to describe the elementary electrochemical reaction mechanisms under transient conditions in polyelectrolyte membrane fuel cell (PEFC) environments. Their nanoscale interfacial model postulates an inner layer formed by dynamically competing surface-adsorbed water molecules and electrochemical intermediate reaction species, which modify the effective water dipolar density and the dynamic evolution of the generated electric potential drop between the metal and the electrolytic phase (i.e., the Frumkin potential across the Stern layer). The inner-layer model is coupled to the standard Poisson-Nernst-Planck (PNP) diffuse-layer model for the diffusion and electro-migration of protons in the presence of fixed counterions representing the PEFC Nafion sulfonate groups. Numerical solutions of this model have shown that diffuse-layer effects are essential to describe time-dependent degradation processes in fuel cells.[17-19] In the present article, we develop a simpler analytical model to predict some basic effects of diffuse charge during steady-state operation.

Interestingly, it is sometimes argued (Ref. 20, p. 13989; Ref. 21, p. 1410) that the relevance of the Frumkin correction must be small because the ion concentrations in polymer electrolytes (such as Nafion) are high. Similarly, Wang et al.[22] (p. A1734) argue that "the term $c_{H+}/c_{H+,\infty}$ [the Frumkin correction] can be approximated by unity because the proton concentration is fixed in acid ionomers, [and] high in acid liquid media, and thus essentially constant during the hydrogen oxidation reaction." These arguments are often used to support neglecting the diffuse part of the double layer and thus replacing the potential difference of the compact (Stern) part by the full potential difference from metal to bulk electrolyte. However, as we will argue, even at high ion concentrations, there can still be a significant potential difference (and proton concentration gradient) in the diffuse part of the polarization layer, which affects reaction rates; as a result, diffuse-charge effects can be important even in solid electrolytes. Similar conclusions have been reached by Franco et al.[10,16] on the basis of nanoscale modeling of PEFCs and by Bazant et al.[14] and Chu and Bazant[15] through analysis of a general mathematical model for binary electrochemical cells. Atomistic calculations also highlight the importance for accounting for diffuse layer effects for a more accurate prediction of the energetics in general interfacial electrochemical processes.[23]

The goal of the present contribution is to derive simple analytical expressions for the voltage and power generated by a fuel cell in steady state, taking into account diffuse charge in the membrane. The physical insights and general formulas resulting from this approach are intended to complement the more detailed time-dependent numerical models of fuel cells described elsewhere (e.g., by Franco et al.[10,16] and references therein). To keep matters as
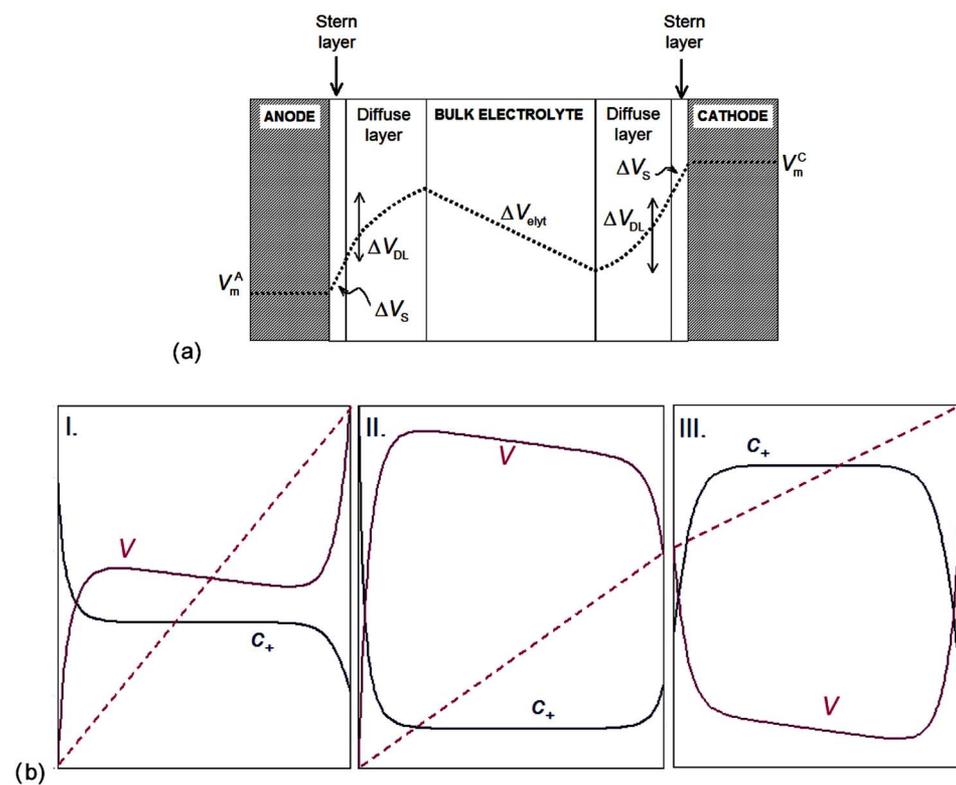
Figure 1. (Color online) (a) Schematic representation of the electrostatic potential profile in the fuel cell membrane. In this representation, there is an excess of protons in the anodic polarization layer and a deficit on the cathodic side. (b) As in (a), but for three cases: I, as in (a); II, with an excess of protons on both sides; and III, with a deficit of protons on both sides. The dashed lines show the electrical voltage increase through the external circuit.

simple as possible, we analyze a planar proton-conducting polyelectrolyte membrane with fixed negative charge.[24] Our analysis is based on two types of mean-field, continuum models for proton transport, where either positive point charges or solvated protons of a nonzero size move in a uniform background density of immobile anions.[11-13] The membrane model is completed by Frumkin-corrected BV reaction kinetics for the charge transfer from the metal catalyst across a uniform Stern layer to the reaction plane. Although this general model already incorporates a number of complicated physical effects, it remains simple enough for mathematical analysis of various limiting cases. In the context of fuel cell modeling, one aspect is the inclusion of ion volume constraints in the description of the polarization layer and the charge transfer rate.

To illustrate the use of the analytical membrane model, we apply it to the simplest case of a fuel cell where the only reactive gas-phase species is hydrogen. In such a "concentration cell," it is a difference in hydrogen concentration between the anodic and cathodic compartments that drives the electrical current.[25] This allows us to neglect other processes, such as the catalytic conversion of gaseous oxygen, and to consider only the Tafel–Heyrovsky–Volmer reaction mechanism for the conversion of molecular hydrogen into protons and electrons at each electrode.[10,20,21] As a first approximation, we neglect the Heyrovsky reaction step, which is a mixed reaction of simultaneous atomic hydrogen adsorption and proton formation. Transport limitations in the gas phases, nonisothermal operation, and the nonzero thickness of the electrode reaction region (and the mass transport therein[26]) are also neglected, as well as water transport for the case of PEFCs.[27] Although we consider the adsorption/desorption equilibrium of hydrogen onto the catalyst, we neglect a diffusional limitation for the adsorbed hydrogen atoms on the catalyst surface. In summary, we consider as possible rate-limiting steps the ad-/desorption of hydrogen, the electrochemical conversion of hydrogen atoms into protons (and vice versa), as well as the ohmic transport of electrons and ions through the external circuit and the electrolyte membrane, respectively. Although our analysis is performed for a hydrogen concentration cell, it can easily

be extended to other types of fuel cells or electrochemical systems, and its conclusions about diffuse-charge effects on reaction rates should have broad applicability.

Theory

As explained above, we illustrate the modeling of diffuse charge in a fuel cell membrane via the example of an electrochemical hydrogen concentration cell, where the only mobile and reactive ion in the electrolyte phase is the proton. At the cathode, the proton can react with an electron to form a neutral adsorbed hydrogen atom (Volmer reaction step) that can diffuse over the catalytic surface, combine with a second hydrogen atom, and desorb as molecular hydrogen (Tafel reaction step). We assume that the adsorbed hydrogen atoms are at equilibrium with the hydrogen molecules. For simplicity, we neglect a possible limitation in the catalytic surface concentration of sites for protons to adsorb to (i.e., we set the adsorption site vacancy concentration θ_s to unity[16]). At the anode, we have the reverse situation.

Ohmic laws.— According to Ohm's law, the generated electrical voltage, V, is given by

$$V = V_{C,m} - V_{A,m} = iR_{ext} \qquad [1]$$

with i is current, R_{ext} is the external resistance, and $V_{C,m}$ and $V_{A,m}$ are the electrical potentials in the metallic phase of the cathode and anode, respectively. In the electrolyte bulk phase (membrane), we also assume Ohm's law[13]

$$\Delta V_{elyt} = V_{A,b} - V_{C,b} = iR_{elyt} \qquad [2]$$

where b stands for the electrolyte bulk phase, just beyond the polarization layer (outer, or Volta, potential), and where the electrolyte resistance is given for a planar membrane by

$$R_{elyt} = \frac{L}{A\sigma} \qquad [3]$$

where L is the thickness, A is the area, and σ is the ionic conductivity of the membrane. Assuming that protons are the only charge-carrying ions, σ is given by

$$\sigma = Dc_\infty \frac{e^2}{kT} \qquad [4]$$

where D is the proton diffusion coefficient and c_∞ is the bulk proton concentration.

BV equation.— The BV equation including the Frumkin correction describes the electronic current at the electrode-electrolyte interface as the sum of a cathodic and an anodic reaction[2,3,6-19]

$$i = -k_R c_O \exp(-\alpha_R f \Delta V_S) + k_O c_R \exp(\alpha_O f \Delta V_S) \qquad [5]$$

where k_R and k_O are reaction rate constants, c_O and c_R are concentrations at the reaction plane of the ion in the oxidized (O) and reduced (R) state, and ΔV_S is the Stern potential difference, defined as the difference in potential between the metal phase (the electrode), $V_{j,m}$, and the potential at the reaction plane, V_r, thus $\Delta V_S = V_{j,m} - V_r$. The sum of the transfer coefficients α_R and α_O equals unity; f equals F/RT, or e/k_BT. We stress that if diffuse charge were neglected, as in most fuel cell models, the Stern potential drop ΔV_S would be replaced by the total voltage drop across the full double layer, from the metal to the neutral bulk phase.

The representation of Eq. 5 considers both the oxidant and reductant to be species present in the electrolyte phase (typical for an electrochemical reaction in a polar solvent, such as water). However, in fuel cells, one of the species that participates in the electrochemical reaction is typically uncharged and derives from an adjacent phase (such as the hydrogen atoms that are surface adsorbed to a catalytically active surface), and it is a standard approximation to set its concentration near the site of the electrochemical reaction equal to the reactant concentration c_O or c_R in Eq. 5. As discussed below, Eq. 5 also assumes an ideal dilute solution, which can be relaxed more generally by replacing concentrations with chemical activities. Further on, we consider corrections due to excluded volume of the reacting species in the electrolyte phase.

The sign of the current i in Eq. 5 is defined to be negative at the cathode (i.e., negative in the direction for reduction, $O^+ + e^- \rightarrow R$). Implementing in Eq. 5 the proton for O, the adsorbed hydrogen atom for R, and assuming that the electron transfer coefficients are given by $\alpha_O = \alpha_R = 1/2$, we obtain the Volmer reaction rate for the electrochemical conversion of hydrogen

$$i = -k_R c_{H^+} \exp\left(-\frac{1}{2}f\Delta V_S\right) + k_O c_{H_{ads}} \exp\left(\frac{1}{2}f\Delta V_S\right) \qquad [6]$$

We can relate the concentration of adsorbed hydrogen atoms $c_{H_{ads}}$ to the gas-phase hydrogen pressure p_{H_2} according to the Tafel reaction step[10]

$$i = k_{ads}p_{H_2} - k_{des}c_{H_{ads}}^2 \qquad [7]$$

We now make two simplifications: (*i*) Assuming that the ad/desorption of hydrogen gas in Eq. 7 is fast compared to the faradaic reactions at both electrodes in Eq. 6, the adsorbed hydrogen atom is in equilibrium with the molecular hydrogen, and we can replace $c_{H_{ads}}$ in Eq. 6 by $\sqrt{k_{ads}/k_{des} \cdot p_{H_2}}$ and define $k_j = k_O \cdot \sqrt{k_{ads}/k_{des}}$; (*ii*) For thin double layers and non-negligible bulk ion concentrations, it is common to assume local electrochemical equilibrium, or a constant electrochemical potential, in the diffuse layers in the electrolyte. Ignoring volume constraints for a dilute solution, this allows us to relate the concentration of protons at the reaction plane, c_{H^+}, to the proton concentration in the bulk of the electrolyte phase, c_∞, according to a Boltzmann distribution

$$c_{H^+} = c_\infty \exp(-f\Delta V_{DL}) \qquad [8]$$

where the potential difference across the diffuse part of the double layer is ΔV_{DL}, which is $V_r - V_b$. In the bulk electrolyte phase, the proton concentration is approximately constant and at a value of c_∞, which equals the concentration of the background, fixed, negative charge. This has previously been shown by Franco et al.[10] by solving the full PNP equations for the transport of protons in Nafion, a polyelectrolyte membrane, where the thickness of the polarization layer was found to be between 1 and 5 nm for the anode and cathode diffuse layers in a PEFC. The nearly uniform bulk proton concentration due to fixed anions is a crucial difference between solid and liquid electrolytes, which eliminates diffusion limitations and nonequilibrium space-charge formation;[15] instead, bulk transport is dominated by electromigration and the diffuse layers typically remain in equilibrium. With these two simplifications, Eq. 6 takes the form

$$i = -k_j\left\{\sqrt{p^*} \exp\left(-f\Delta V_{DL} - \frac{1}{2}f\Delta V_S\right) - \sqrt{p_{H_2}} \exp\left(\frac{1}{2}f\Delta V_S\right)\right\} \qquad [9]$$

where

$$\sqrt{p^*} = c_\infty \frac{k_R}{k_j} \qquad [10]$$

The critical fuel pressure p^* is a thermodynamic constant of the fuel cell membrane at given temperature, and k_j is a kinetic constant dependent on structural details of the electrode.

Structure of the polarization layers.— Let us discuss the structure of the Stern and diffuse layer in more detail. Directly next to the electrode is the charge-free Stern layer, across which the potential decay is ΔV_S, which is separated by the reaction plane from the diffuse layer (or "space-charge region"), across which the potential drop is $\Delta V_{DL} = V_r - V_{j,b}$, where DL stands for diffuse layer. The reaction plane is located within the electrolyte phase, and is the closest interface to where the reacting ions and atoms that are in the electrolyte phase are assumed to be able to approach the metallic phase. The reaction plane is often denoted as the "outer Helmholtz plane" or "Stern plane." (We can also interpret it as the typical distance over which the electron can tunnel from electrode into the electrolyte; Ref. 2, p. 130). In the diffuse layer, both the proton concentration and the electric potential rapidly change. For ideal Boltzmann–Coulomb statistics based on Eq. 5, the structure of the diffuse layer is described by the Poisson–Boltzmann (PB) equation, which amounts to a mean-field approximation for pointlike ions. However, many modified theories are available that incorporate correlations or excluded volume effects.[28,29]

To relate the potential drop over the Stern layer ΔV_S to the charge stored in the diffuse layer, q (in charge/area), we consider continuity of the electrical displacement at the reaction plane, assuming a constant electric field in the Stern layer, to obtain

$$q = -\varepsilon\frac{\Delta V_S}{\lambda_S} \qquad [11]$$

which is identical to the calculation of the nondipolar contribution $\Delta\varphi_1$ to the overall Frumkin potential difference, given in Franco et al.[16] This is a standard approximation, which (via Gauss' law) relates the Stern voltage drop to the normal electric field at the inner edge of the diffuse layer, by modeling the Stern layer as a thin, planar, dielectric film. Equation 11 provides a boundary condition for the electrostatic potential whenever diffuse charge is considered.[9,14,30] In Eq. 11, the parameter λ_S is an effective width for the Stern layer, equal to its true width times the permittivity ratio of the electrolyte to the Stern layer, and ε is the permittivity of the electrolyte, which relates to κ, the inverse Debye length, and to c_∞, the background number concentration of negative charge, according to $\kappa^2 = 2c_\infty e^2/(\varepsilon k_B T)$. For our purposes, Eq. 11 amounts to the as-
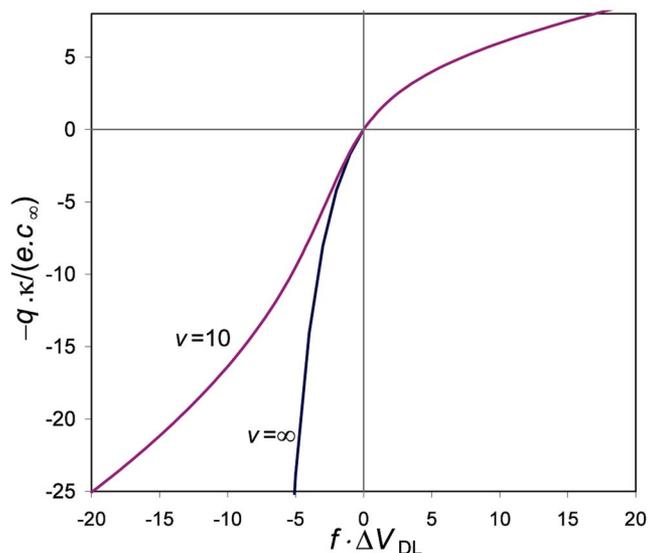
Figure 2. (Color online) Surface charge density q of the polarization layer as a function of diffuse-layer potential difference ΔV_{DL} according to the modified one-dimensional planar PB model with fixed anions and mobile cations, as function of volume parameter v, which is the inverse volume fraction of protons in the bulk phase.

sumption of a constant Stern-layer capacitance, which can be relaxed and extended in various ways, as discussed in Ref. 14 and 16.

To calculate the total charge (per unit area) stored in each diffuse layer, q, we must consider the detailed structure of these layers, including the concentration of fixed counter charge, and we require a model for the electrostatic potential. For an ideal, dilute solution in equilibrium, the standard model is based on PB theory, which is a mean-field approximation for pointlike ions, as noted above. In the simplest case of a symmetric binary electrolyte, Gouy's solution to the PB equation yields Chapman's well-known formula

$$q = -4ec_\infty\kappa^{-1}\sinh\left(\frac{1}{2}\Delta V_{DL}\right) \qquad [12]$$

but this is not suitable for a solid electrolyte, with only one mobile species. Instead, we must solve the PB equation for mobile protons, and for anions which are fixed (to a good approximation for most proton-conducting membranes), which results in $2f d^2V/dx^2 = \kappa^2[1 - \exp(-fV)]$. For this case, an analytical formula for the charge density is available, given by[13]

$$q = -2\,\text{sgn}(\Delta V_{DL})ec_\infty\kappa^{-1}\sqrt{\exp(-f\Delta V_{DL}) + f\Delta V_{DL} - 1} \quad [13]$$

where sgn stands for "sign of" [i.e., $\text{sgn}(x) = x/|x|$]. For very negative values of ΔV_{DL}, Eq. 12 and 13 coincide, but for $f\Delta V_{DL}$ close to zero, q as predicted by Eq. 13 is a factor of $\sqrt{2}$ smaller than according to Eq. 12. Because coion expulsion is not considered in Eq. 13, it is more realistic for a solid electrolyte. While for a binary liquid electrolyte, Eq. 12 is symmetric and exponentially diverging in ΔV_{DL}, for a solid electrolyte with only one mobile ion and for $\Delta V_{DL} > 0$ the charge density q as predicted by Eq. 13 grows much more slowly, following a square-root dependence on ΔV_{DL}, which is due to the finite maximum charge density set by the anions (see Fig. 2). Interestingly, analogous models of ionic volume constraints in a binary electrolyte[28] or molten salt[31] yield the same square-root scaling at both large positive or negative voltage, because in all these cases, the diffuse layer has asymptotically uniform charge density set by the maximum density of counterions. For a solid electrolyte, the strong asymmetry of the total charge density with voltage is a very interesting aspect of polarization layers that have fixed back-

ground charge, whose role in fuel cell membranes has not previously been discussed.

One assumption behind Eq. 13 is that the protons in the electrolyte are point charges. However, the finite volume of the protons can be taken into account in various ways, while maintaining the mean-field approximation, following the classical theory of steric effects in a binary electrolyte.[28,32,33] The simplest approach is based on a Langmuir lattice isotherm, where the controlling parameter, v, is the number of available sites per proton ($v > 1$) in the quasi-neutral bulk phase. Equivalently, the parameter $\phi_\infty = 1/v$ is the volume fraction occupied by protons in bulk (analogous to the parameter ν defined in Ref. 28). For a model of a solid electrolyte with one mobile ion of finite size, Itskovich et al. derived a modified form of the charge-voltage relation[11]

$$q = -2\,\text{sgn}(\Delta V_{DL})ec_\infty\kappa^{-1}$$
$$\times \sqrt{f\Delta V_{DL} + v\,\ln\{1 + v^{-1}[\exp(-f\Delta V_{DL}) - 1]\}} \quad [14]$$

which reduces to Eq. 13 for very large v. The volume constraint on the proton concentration leads to the same square-root asymptotic scaling of the total charge with diffuse-layer voltage for a positively charged diffuse layer ($\Delta V_{DL} < 0$), as that noted above for a negatively charged diffuse layer ($\Delta V_{DL} > 0$), because in both limits the charge density becomes saturated at finite limiting values. In Fig. 2, we give results for q vs ΔV_{DL} using Eq. 13 (when v is set to infinity) and using Eq. 14 (setting $v = 10$), where these general trends are apparent.

Steady-state electrical potential profiles.— Figure 1a shows a schematic representation of the potential profiles in the electrochemical cell model. Here, an example is given with an excess of protons in the anode polarization layer, related to the fact that the diffuse layer potential difference ΔV_{DL} is negative [ΔV_{DL} being the difference in potential at the Stern plane (reaction plane) relative to the value in the bulk electrolyte]. On the cathode side, we have a deficit of protons and $\Delta V_{DL} > 0$. Because we assume local equilibrium in the double layer, the Stern layer potential difference ΔV_S always has the same sign as the diffuse-layer potential difference because the electric displacement is continuous at the Stern plane. Though we expect this approximation to have broad applicability for fuel cell membranes, it is important to note that at a large enough current, or for a too weak diffuse-layer field, local equilibrium can be violated, which can cause "charge inversion" in the diffuse layer, as has recently been predicted using a similar mean-field model for biological membranes transmitting ionic current.[34]

In our model of a fuel cell membrane, the magnitudes of $\Delta V_{DL,i}$ and $\Delta V_{S,i}$ are coupled through Eq. 11 in combination with either Eq. 12, 13, or 14. The electric potential decreases through the bulk of the electrolyte (thus, $\Delta V_{elyt} = V_{A,b} - V_{C,b} > 0$), which is a required condition for the protons to spontaneously migrate in the electric field through the bulk electrolyte. Similarly, the external potential difference $\Delta V_{ext} = V_{m,C} - V_{m,A}$ must be positive for the electrons to flow spontaneously through the external circuit and do work. Now it is important to realize that though ΔV_{ext} and ΔV_{elyt} must always be positive, the polarization layer potential differences $\Delta V_{DL,i}$ and $\Delta V_{S,i}$ do not necessarily have the signs as depicted in Fig. 1a, with the associated excess of protons on the anode side and a proton deficit on the cathode side. Actually, we can have the situation that both layers have a deficit of protons, or both have a proton excess (see cases II and III in Fig. 1b). This situation, for instance, occurs when the current is low and both gas-phase pressures (at the anode side and at the cathode side) are above p^* (resulting in an excess of protons on both sides), or when both gas-phase pressures are below p^* (resulting in a proton deficit on both sides). However, other parameter settings are also possible to give these "symmetric" situations.

The case of a proton deficit on the anode side, and an excess on the cathode side, is impossible within our model. This can be concluded from the fact that the potential must be continuous through

the entire circuit (see Eq. 29 below) and that ΔV_{elyt} and ΔV_{ext} must always be positive. Roughly speaking, the two polarization layers (each consisting of a diffuse part plus a Stern part) must "rectify" the potential mismatch created in the system by the bulk proton transport and the external electron transport. Therefore, the two polarization layers must compensate for the total potential drop ΔV_{elyt} plus ΔV_{ext}. This is most effectively done when having an excess of protons on the anode side and a deficit on the cathode side, but Kirchoff's rule of zero total voltage drop around a current loop (Eq. 29) can also be respected in a system where there is an excess of protons on both sides, or a deficit of protons on both sides, as illustrated in Fig. 1b.

We stress again that, in the present model, the excess proton charge on the anodic side is not constrained in any way to exactly compensate the proton charge deficit on the cathodic side. The total diffuse charge on the membrane (number of mobile protons minus the number of fixed anions) though generally small (compared to the total number of ions) typically is nonzero. This violation of the traditional assumption of overall electroneutrality of the membrane, due to unbalanced diffuse charge produced by the faradaic reactions, has been explicitly noted and quantified in models of binary electrochemical thin films[14] while in the context of fuel cell membranes is implicitly included in the model of Ref. 10.

Influence of ion volume constraints on the electrochemical charge transfer rate.— A fundamental question that has received little attention in the electrochemical literature is the manner in which nonideal solution behavior at an interface affects faradaic reaction rates, going beyond the BV equation (Eq. 5). For example, above we have accounted for volume constraints in the solid electrolyte at equilibrium following a classical lattice-gas model, but there are two basic ways that such entropic considerations should also influence the reaction rate: (*i*) the ion concentration at the reaction (Stern) plane, relative to the bulk, is altered by steric effects in the diffuse layer, and (*ii*) the reaction kinetics may be directly affected by volume constraints on the reactants and activated complexes, thus modifying the local BV equation (Eq. 5).

Effect (*i*) follows from the equilibrium theory for the polarization layer given by Eq. 11 and 14. Using a lattice-based model of volume constraints, the equilibrium distribution (Eq. 8) must be modified by adding to the ideal chemical potential an excess term given by $\mu^{ex} = -\ln(1 - \phi)$, where $\phi = c/(c_\infty v)$ is the excluded volume.[13,28,32,33] The approximation of constant electrochemical potential then yields the proton concentration at the reaction plane, to be used in Eq. 6

$$c_{H^+} = c_\infty \frac{1 - \phi}{1 - \phi_\infty} \exp(- f\Delta V_{DL}) = c_\infty \frac{v \exp(- f\Delta V_{DL})}{v - 1 + \exp(- f\Delta V_{DL})}$$
[15]

which resembles a Fermi–Dirac distribution and reduces to the Boltzmann distribution (Eq. 8) in the limit $v \to \infty$. In the opposite limit $v \to 1$, the proton concentration at the Stern plane approaches the value in bulk (i.e., $c_{H^+} \to c_\infty$) because volume constraints are so strong that protons remain at a nearly uniform concentration of "close packing" across the entire membrane.

Effect (*ii*) can be included in various ways. A general approach, consistent with the treatment of the bulk, is to express reaction rates in terms of differences in chemical potential for the reaction complex, as it undergoes stochastic transitions in a landscape of excess chemical potential (relative to an ideal gas). Such a theoretical framework is developed in Ref. 35 and applied there to various examples of surface adsorption and electrochemical reactions in concentrated solutions. One example can be found in Ref. 36, where the intercalation reaction in a rechargeable battery cathode is driven by changes in chemical potential, which include contributions from differences in enthalpy, entropy, and concentration gradients, in a general lattice-based phase-field model.

Here, we apply the more familiar approach to describe volume constraints in reactions, similar to Langmuir-isotherm models for

specific adsorption of ions on electrodes,[1] although we focus on the reverse situation, where volume constraints arise only in the electrolyte phase, consistent with our electrolyte membrane model, and not for the adsorbed neutral hydrogen atoms on the catalyst surface. As in standard models of heterogeneous catalysis, the reaction plane is conceptually divided into a lattice of sites, where both occupied and unoccupied sites are considered as reacting species. The true reaction $O + e^- \leftrightarrow R$ occurring in a concentrated solution is thus replaced by the approximate dilute-solution reaction, $O + e^- + S \leftrightarrow R$, where S is a vacant site for the ion O in the oxidized state. This reduces the oxidation reaction rate by a factor $1 - \phi$, which is the available volume fraction in the reaction plane for new protons resulting from oxidation of hydrogen. We ignore volume constraints in the reverse reaction rate [except for effect (*i*) above] by assuming that the occupancy of adsorbed neutral hydrogen atoms on the catalyst surface remains small enough not to hinder the reduction of protons.

Including these two effects in the BV equation (Eq. 6) results in

$$i = -(1 - \phi)\left\{ k_R \frac{c_\infty}{1 - \phi_\infty} \exp\left(- f\Delta V_{DL} - \frac{1}{2} f\Delta V_S\right) \right.$$
$$\left. - k_O c_{H_{ads}} \exp\left(\frac{1}{2} f\Delta V_S\right) \right\}$$
[16]

which can be simplified to

$$i = -k_j(1 - \phi)\left[\sqrt{p^*} \exp\left(- f\Delta V_{DL} - \frac{1}{2} f\Delta V_S\right) \right.$$
$$\left. - \sqrt{p_{H_2}} \exp\left(\frac{1}{2} f\Delta V_S\right) \right]$$
[17]

where we assume infinitely fast hydrogen ad-/desorption (the Tafel reaction step) and where the critical pressure p^* is slightly modified via $\sqrt{p^*} = c_\infty/(1 - \phi_\infty) \cdot k_R/k_j$. In summary, when proton volume constraints are incorporated in the membrane model, we suggest that Eq. 9 is modified by a prefactor $1 - \phi$, where ϕ follows from $\phi = c_{H^+}/(c_\infty v)$ with c_{H^+} from Eq. 15, and by the replacement of the constant c_∞ by $c_\infty/(1 - \phi_\infty)$. Furthermore, ΔV_{DL} and ΔV_S are no longer related to each other through Eq. 11 and 13, but require Eq. 11 and 14.

Results and Discussion

In this section, numerical results are presented for the concentration cell model, and simple analytical results are derived for several limits. The critical hydrogen pressure p^* defined above is the same at both electrodes because it is a thermodynamic parameter for the membrane electrolyte material. First, we derive simple formulas for an ideal, dilute membrane, and then we consider effects of volume constraints at high proton concentrations.

Analytical solution for $p_{H_2,A} = p_{H_2,C}$.— We begin by considering the equilibrium situation, where the gas-phase hydrogen pressure p_{H_2} is equal on both sides of the membrane, and no current flows. Setting $i = 0$ in Eq. 9, we obtain

$$\sqrt{p^*} \exp(- f\Delta V_{DL}) = \sqrt{p_{H_2}} \exp(f\Delta V_S)$$
[18]

which, using Eq. 11 and 13, yields the nonlinear relation

$$f\Delta V_S = \text{sgn}(\Delta V_{DL})\delta \sqrt{\exp(- f\Delta V_{DL}) + f\Delta V_{DL} - 1}$$
$$\sim \frac{1}{\sqrt{2}}\delta\left[f\Delta V_{DL} - \frac{1}{6}(f\Delta V_{DL})^2 + \cdots \right]$$
[19]

which can be solved iteratively. Following Ref. 9, 14, and 32, we have introduced the dimensionless parameter $\delta = \lambda_S\kappa$, the ratio of the effective Stern-layer thickness to the diffuse-layer thickness, because this allows us to analyze the limits of large and small polarization effects. Note that combination of Eq. 11 with Eq. 12, 13, or 14 results in a relation between ΔV_S and ΔV_{DL} which only depends

on δ and f and does not require values for κ or c_∞.

For a sufficiently high gas-phase hydrogen pressure some of the hydrogen molecules will be converted into excess protons residing in the electrolyte (with the electrons stored on the surface of the metal phase). As the gas-phase pressure is decreased, below a certain p_{H_2} there is no longer an excess of protons in the material, but instead a proton deficit will develop (i.e., the polarization layers become negatively charged). Let us first find the value of p_{H_2} for which the total excess proton charge in the electrolyte is zero (i.e., the gas phase pressure for which the electrolyte membrane is uncharged). In this case, $q = 0$, thus also ΔV_{DL}, as well as ΔV_S. Inserting $\Delta V_{DL} = \Delta V_S = 0$ in Eq. 18, we obtain the result that $p_{H_2} = p^*$. Therefore, at an applied hydrogen pressure of p^*, the membrane has zero total charge. At this special pressure, no molecules are taken up or released by the material; thus, it is meaningful to view p^* as a thermodynamic property of the electrolyte material, in equilibrium with hydrogen gas.

For any other gas conditions, the total charge on the electrolyte will generally be nonzero, in contrast to traditional membrane models assuming electroneutrality. The total charge can be cumbersome to calculate analytically, but close to $p_{H_2} = p^*$ we can use the linearization of ΔV_S vs ΔV_{DL} as given by Eq. 19. Together with Eq. 11 this results in

$$q = ec_\infty \kappa^{-1} (\delta + \sqrt{2})^{-1} \ln \frac{p_{H_2}}{p^*} \qquad [20]$$

which shows that for $p_{H_2} > p^*$ the electrolyte will become positively charged (containing an excess of protons in both polarization layers), and vice versa for $p_{H_2} < p^*$. Equation 20 suggests that physical parameters of the electrolyte material, such as p^* or δ, can be inferred from experimental measurements of stored charge vs applied pressure, in equilibrium.

The above analysis shows that when diffuse-layer polarization is included in the membrane model, it can naturally describe the total proton charge stored in the polarization layers, even at equilibrium (e.g., as function of the gas-phase hydrogen pressure). In contrast, when diffuse-layer effects are omitted, polarization charge is absent from the model and assumed to be zero. Indeed, it is commonly believed that the stored charge in the membrane (via its differential capacity C_{DL}) is only relevant for dynamical modeling of fuel cells via resistor-capacitor (RC) circuit models. We stress, however, that the standard BV approach does not give a rationale for the existence or relevance of C_{DL}, and its widespread use in empirical RC models for transients in fuel cells is thus theoretically inconsistent. Instead, the Frumkin-corrected BV equation naturally includes the polarization layer capacity C_{DL}, and shows that C_{DL} is not only important for transients, but also for stationary operation, and even for equilibrium.

Simplified model for very high kinetic rates.— Next we consider a concentration cell operating in a steady state, with $p_{H_2,A} > p_{H_2,C}$. In the case that the electrochemical kinetics are very fast (as well as the hydrogen ad-/desorption step), the equilibrium Eq. 18 is valid at both electrodes, and together with Eq. 1, 2, and 29 (to be discussed further on), we obtain for the cell voltage vs current i the well-known expression

$$V = V_0 - iR_{elyt} \qquad [21]$$

where the ideal Nernstian cell voltage V_0 is given by

$$V_0 = \frac{1}{2f} \ln \frac{p_{H_2,A}}{p_{H_2,C}} \qquad [22]$$

The generated electrical power ($P = iV$) is then straightforwardly derived from Eq. 1 and 21. As Eq. 21 shows, for infinitely fast kinetics, the details of charge stored in the polarization layers, as described by Eq. 19, are irrelevant. In this respect, the present model behaves as expected.

Simplified model for electrochemical kinetic rates very high.— Next we consider the case where the electrochemical step (Volmer) is still very fast (i.e., at equilibrium), but a limited rate for the hydrogen ad-/desorption (Tafel) is considered. The electrochemical reaction equilibria follow from Eq. 6, assuming that both the oxidation and reduction rates are much larger than the current i, and thus equal to one another. This determines the total double-layer voltage on each electrode

$$\Delta V_T = \frac{1}{2f} \ln \left(\frac{p^*}{c_{H_{ads,j}}^2} \frac{k_{ads,j}}{k_{des,j}} \right) \qquad [23]$$

where $\Delta V_T = \Delta V_S + \Delta V_{DL}$. In this case, Eq. 21 is modified to

$$V = \frac{1}{2f} \ln \left(\frac{k_{ads,C}}{k_{ads,A}} \frac{k_{ads,A}p_{H_2,A} - i}{k_{ads,C}p_{H_2,C} + i} \right) - iR_{elyt} \qquad [24]$$

For a very small current i [due to a high value of R_{ext} (i.e., close to an open circuit)], or a high value for $k_{ads,A}$ and $k_{ads,C}$, Eq. 24 reduces to Eq. 21 and 22. For a very low external resistance R_{ext} (close to a short circuit), $V \to 0$ and the (maximum) current i is obtained iteratively from Eq. 24. Setting $R_{elyt} = 0$ and $k_{ads,A} = k_{ads,C}$, we obtain a simple analytical result for the maximum current, $i_{max} = 1/2 \cdot k_{ads}(p_{H_2,A}-p_{H_2,C})$, which is an example of a "reaction-limited current," also predicted in some regimes for binary electrochemical thin films.[8,10]

Thus, when only the electrolyte resistance and the hydrogen ad-/desorption kinetics are important, the details of the polarization layers are unimportant for steady-state behavior. Clearly, for diffuse layer effects to play a role in the steady state, the electrochemical reaction must be at least partially rate limiting, which we consider next. For simplicity, we will assume hereafter that the hydrogen ad-/desorption reaction (Tafel reaction step) is always at equilibrium, so that we can use Eq. 9 for both the anode and the cathode. At the end of this section, we will include volume effects and will replace Eq. 9 by Eq. 17.

Helmholtz and GC limits.— In the general situation where electrochemical reactions are at least partially rate limiting, simple analytical results are possible in two interesting limits, namely, where the effective Stern layer thickness λ_S is either much larger or much smaller than the diffuse-layer thickness κ^{-1}. In the former "Helmholtz limit," $\delta \to \infty$ and $\Delta V_S \gg \Delta V_{DL}$, and the Stern layer carries the total double-layer voltage and diffuse-layer polarization is zero. In the latter "Gouy–Chapman (GC) limit," $\delta \to 0$ and $\Delta V_S \ll \Delta V_{DL}$, and the Stern potential difference can be set to zero. These asymptotic limits based on the parameter δ were introduced in Ref. 14 in the context of modeling binary-electrolyte thin films; here, we develop a similar analysis for a fuel cell membrane.

Combining Eqs. 2, 9, and 29 and setting $\Delta V_{DL,j} = 0$ results for the Helmholtz limit in an explicit expression for the generated voltage V versus the current i given by

$$V = V_0 - \left\{ \frac{2}{f} \text{arcsinh} \frac{i}{2k_A \sqrt[4]{p^* p_{H_2,A}}} + iR_{elyt} \right. $$
$$\left. + \frac{2}{f} \text{arcsinh} \frac{i}{2k_C \sqrt[4]{p^* p_{H_2,C}}} \right\} \qquad [25]$$

This formula resembles standard expressions from fuel-cell models assuming a neutral membrane and BV kinetics, if we identify $k_j \sqrt[4]{p^* p_{H_2,j}}$ as the exchange current density i^*. Indeed, in standard BV fuel cell modeling,[4,37-44] the ideal voltage V_0 is reduced (as in Eq. 25) by subtracting the ohmic drop across the electrolyte, iR_{elyt}, and the surface overpotential $\eta = 2/f \cdot \text{arcsinh}(i/2i^*)$ for each electrode. In all of these fuel cell models, the Tafel and Heyrovsky reaction steps are neglected, just as in the present model. For low currents i, Eq. 25 simplifies to

$$V = V_0 - i \cdot \left[(fk_A \sqrt[4]{p^* p_{H_2,A}})^{-1} + R_{elyt} + (fk_C \sqrt[4]{p^* p_{H_2,C}})^{-1} \right]$$

$$[26]$$

which has the familiar form of two "charge-transfer resistances" in series with the electrolyte bulk resistance, R_{elyt}. The charge-transfer resistance in Eq. 26 scales with hydrogen pressure to power $-1/4$ (see also Table III in Ref. 42).

The analysis shows that the state-of-the-art BV models in literature can be identified as the Helmholtz limit ($\delta \rightarrow \infty$) of our more complete model, resulting in Eq. 25. This identification makes it possible to systematically extend the state-of-the-art approach to BV modeling to allow for nonzero membrane charge by taking finite values of δ instead of implicitly assuming $\delta \rightarrow \infty$.

Departures from electroneutrality are most important in the GC limit, $\delta = 0$; thus, this limit is convenient to quantify maximum effects of diffuse charge using our model. Assuming $\Delta V_S = 0$ in Eq. 9, we obtain an explicit expression for the generated voltage V as function of the current i given by

$$V = V_0 - \left\{ f^{-1} \ln\left(\frac{k_A \sqrt{p_{H_2,A}}}{k_A \sqrt{p_{H_2,A}} - i} \right) + iR_{elyt} \right.$$
$$\left. + f^{-1} \ln\left(\frac{k_C \sqrt{p_{H_2,C}} + i}{k_C \sqrt{p_{H_2,C}}} \right) \right\}$$
$$[27]$$

which has different nonlinear, surface-overpotential contributions compared to the opposite limit of an uncharged membrane in Eq. 25. For small currents i, Eq. 27 simplifies to

$$V = V_0 - i \cdot \left[(fk_A \sqrt{p_{H_2,A}})^{-1} + R_{elyt} + (fk_C \sqrt{p_{H_2,C}})^{-1} \right] \quad [28]$$

Thus, in the GC limit, we have, just as in the Helmholtz limit, an analytical expression for the linearized current-voltage relation, which corresponds to a "resistances-in-series" model, but with very different expressions for the charge transfer resistance (i.e., compare Eq. 26 to Eq. 28). An interesting point is that the GC limit does not reduce to the same expression as for the Helmholtz limit, even though both limits are independent of details of the polarization layer. This difference is due to the fact that in the GC limit the concentration of ions (protons) in the charge-transfer reaction is evaluated at the Stern reaction plane, while in the Helmholtz limit bulk-phase values are used. Interestingly, the two expressions given above are equally valid for the case of fixed countercharge (as in a solid electrolyte) as for the situation that the countercharge is mobile (as for aqueous solution). It must finally be noted that when Eq. 27 is used outside the fuel cell range (where $0 < V < V_0$), it will diverge at two limiting currents which are $i_{min} = -k_C \sqrt{p_{H_2,C}}$ and $i_{max} = k_A \sqrt{p_{H_2,A}}$.

Electrochemical reactions partially rate limiting—numerical calculations.— To illustrate the behavior of the model in general situations, between the limits analyzed above, we obtain numerical solutions. The complete model is based on Eq. 1, 2, 9, and 19, where Eq. 9 and 19 are evaluated on both the anode and cathode. Equation 9 for the cathode requires an additional minus sign. The model is completed with an overall potential constraint, given by

$$\Delta V_{S,A} + \Delta V_{DL,A} + \Delta V_{elyt} - \Delta V_{DL,C} - \Delta V_{S,C} + \Delta V_{ext} = 0 \quad [29]$$

where ΔV_{ext} is equal to the generated voltage V as used in the above equations. This set of equations is a self-consistent one-dimensional steady-state model, including diffuse-layer effects (but without volume constraints for the protons), in which the hydrogen atom on the catalytic surface is considered to be at equilibrium with the bulk gas phase. In this model, both charge-transfer limitations and bulk-transport limitations within the membrane are considered.

Unless otherwise stated, the parameter settings are $\delta = 1$, $v = \infty$, and $p^* = 10^{-6}$ bar in the examples below. For the electrochemical kinetic constants, we will generally assume $k_j = k = k_A = k_C$ (with dimension A/bar$^{1/2}$). At the anode side the hydrogen pres-
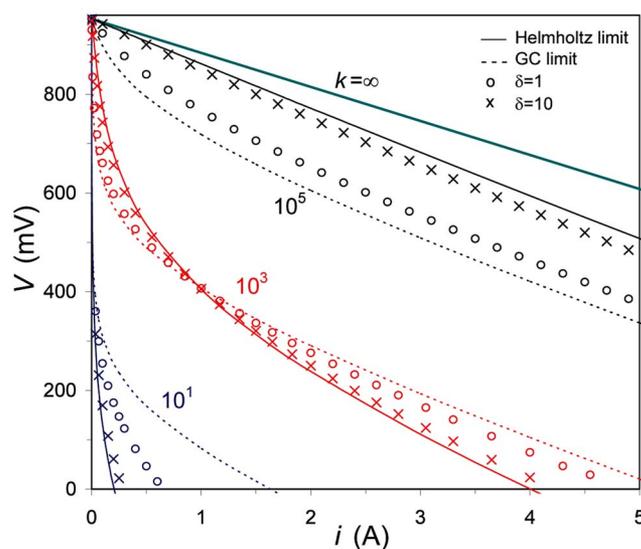

Figure 3. (Color online) Generated voltage V vs current i in a hydrogen concentration cell with a proton-conducting membrane. Parameter values are discussed in the text. k is the kinetic rate constant of both the anode and cathode charge-transfer reaction (with dimension A/bar$^{1/2}$). The case "$k = \infty$" represents absence of kinetic limitation. Symbols represent the numerical model (x: $\delta = 10$; $\bigcirc$: $\delta = 1$), while solid and dashed lines give the Helmholtz and GC limits, respectively.

sure is set to $p_{H_2,A} = 1$ bar, while it is 1 pbar at the cathode ($p_{H_2,C} = 10^{-12}$ bar). The temperature is $T = 800$ K, and thus the factor f is equal to $F/RT = 14.51$ V^{-1}. The open-circuit cell voltage is $V_0 = 1/(2f) \ln(p_{H_2,A}/p_{H_2,C}) \sim 952$ mV.

Though the exact values for the chosen parameter are not very relevant for the objective of the paper (which is to explain the structure of a fuel cell model that includes diffuse-charge effects), we have taken realistic parameter settings: $T = 800$ K is typical for a high-temperature solid-state fuel cell, $V_0 \sim 1$ V is a typical value for an open-circuit voltage, and $p_{H_2,A} = 1$ bar represents atmospheric conditions for the hydrogen gas on the anode side ($p_{H_2,C}$ follows automatically from $p_{H_2,A}$ and V_0). The electrolyte resistance is chosen arbitrary at $R_{elyt} = 68.9$ mΩ, a value that can always be achieved by changing the membrane area or thickness (as long as we can assume that the diffuse layers remain thin). The kinetic rate constant k is varied such that we go from the limit of the purely ohmic transport dominated regime, to parameter settings where the kinetics are rate limiting.

Comparison of full theory with the Helmholtz and GC limits.— We now show that the simple analytical formulas derived above tend to bound the numerical solutions of the complete model and thus may suffice for use in many practical situations. In Fig. 3, we present results for the full theory (symbols are as follows: $\bigcirc$: $\delta = 1$, x: $\delta = 10$) and compare to predictions of the Helmholtz and GC limits, given by Eq. 25 and 27 (solid and dashed lines, respectively). In the limit where kinetic limitations are absent (i.e., $k = \infty$), all models reduce to the simple expression given by Eq. 21, with V decreasing linearly with current i. When finite values are used for the kinetic rate constant, very interesting differences develop between the three approaches. At a relatively high kinetic constant of $k = 10^5$ A/bar$^{1/2}$, we observe that the Helmholtz limit gives the highest prediction for V, after which the numerical results for $\delta = 10$ and 1 follow, with the GC limit giving the lowest prediction for generated voltage V. However, for a value of the kinetic constant which is reduced to $k = 10^3$ A/bar$^{1/2}$, this behavior is significantly modified. The region where $V_H > V_{\delta=10} > V_{\delta=1} > V_{GC}$ is limited from current zero to a current of $i \sim 1$ A. Beyond $i \sim 1$ A, the
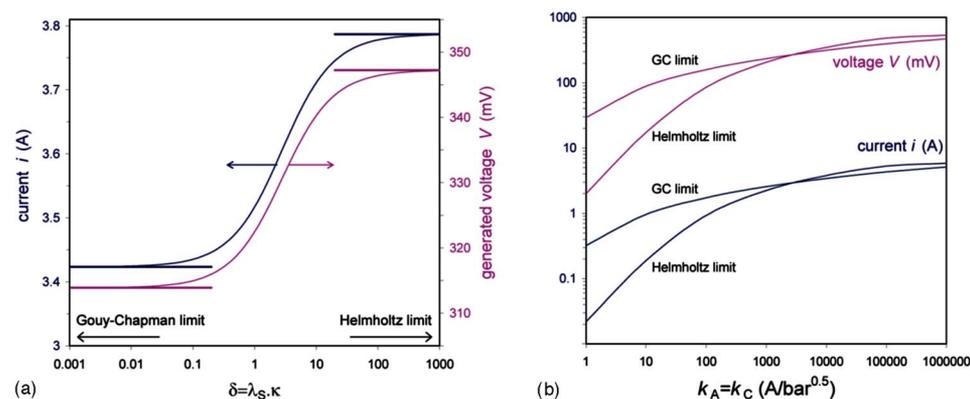
Figure 4. (Color online) Influence of δ, the ratio of Stern layer thickness λ_S to the diffuse-layer thickness, κ^{-1}, on concentration-cell current i and voltage V. (a) Continuous curves are based on full calculations; the Helmholtz limit is based on Eq. 25, and the GC limit on Eq. 27. $k_A = k_C = 10^4$ A/bar$^{1/2}$. (b) Results for i and V in the GC and Helmholtz limit as a function of $k_A = k_C$.

performance sequence is exactly reversed, with V_{GC} higher than predictions of the other calculations. At even lower values of k, the transition point (the value of i above which the GC limit predicts the highest performance) rapidly shifts to zero current (e.g., at $k = 10$ A/bar$^{1/2}$ it is located around $i \sim 0.01$ A). Figure 3 furthermore shows that for the present parameter settings, the Helmholtz limit rather well approximates the exact results if $\delta \geqslant 10$, whereas the GC limit closely follows the exact results for $\delta \leqslant 1$ (except for $k = 10$ A/bar$^{1/2}$ for a current beyond $i \sim 0.2$ A).

In Fig. 4, we analyze the influence of the parameter δ in more detail. For one particular condition given by $k_A = k_C = 10^4$ A/bar$^{1/2}$ and $R_{ext} = 91.6$ mΩ, we give in Fig. 4a results for current i and generated voltage V as function of δ. In this case, both the current i and the concentration cell voltage V increase with increasing δ, while both i and V level off both at very low and very high δ. Furthermore, Fig. 4 shows that the limiting expressions are valid (for this calculation) for $\delta < 0.1$ (for the GC limit) and for $\delta > 100$ (for the Helmholtz limit).

In Fig. 4b, we only analyze the Helmholtz and GC limits and show the influence of the kinetic constant on the prediction of the two limiting expressions. As already observed in Fig. 3, the ratio $\alpha = (i_{GC}/i_H \sim V_{GC}/V_H)$ is a strong function of k, starting significantly above unity at low k (e.g., $\alpha \sim 15$ at $k = 1$ A/bar$^{1/2}$). Thus, at $k = 1$ A/bar$^{1/2}$, we have in the GC-limit currents and voltages that are ~ 15 times higher than in the Helmholtz limit. Increasing k, α decreases, and we have $\alpha = 1$ for $k \sim 3000$ A/bar$^{1/2}$, after which α decreases further to reach a minimum value of ~ 0.82 at $k = 10^5$ A/bar$^{1/2}$. Thus at $k = 10^5$ A/bar$^{1/2}$, predictions for the Helmholtz limit are $\sim 23\%$ above those for the GC limit. With further increasing k, α increases again, finally to reach unity for $k \to \infty$.

Influence of ion volume constraints on reaction rate.— Finally, we analyze the effect of ion volume constraints on the structure of the

polarization layer, the electrochemical reaction rate, and concentration-cell performance. In Fig. 5, we show the influence of $v = 1/\phi_\infty$, where v is the number of potential sites per proton (at the proton bulk concentration), on the voltage difference over the Stern and polarization layer, ΔV_S and ΔV_{DL}, for $\Delta V_T = \Delta V_S + \Delta V_{DL} = -10$ ($\delta = 1$), based on Eq. 11 and 14, while Fig. 6 shows the resulting effect on the cathodic and anodic current (for $k_A = k_C = 1$ A/bar$^{1/2}$). As Fig. 5 shows, for a given ΔV_T, the influence of volume constraints on the Stern and polarization potential differences, as well as on the resulting electrochemical charge transfer rate, can be very large. Whereas without volume constraints, ΔV_S and ΔV_{DL} are about equal in magnitude, when volume constraints are turned on the ratio $\Delta V_{DL}/\Delta V_S$ becomes very large. Simultaneously, the charge transfer rate goes to zero when v goes from infinity to unity.

However, if we run the full concentration cell model (for $k_A = k_C = 10^4$ A/bar$^{1/2}$), we find that at the parameter settings of Fig. 3 there is not such a pronounced influence of volume constraints on cell performance: if we reduce v from $v = 200$ (almost no volume constraints) to $v = 2$ (very significant volume constraints), the generated voltage decreases by a maximum of ~ 90 mV (namely, at high-current, $i \sim 6$ A); see Fig. 6. To increase the influence of volume constraints, we reduce the kinetic rate of the anodic reaction (the anode being the electrode where the protons are typically in excess, which is thus the electrode where volume constraints become most apparent). Reducing k_A by a factor of 10^2 has only a small influence on the generated voltage when $v = 200$, but has a very significant influence when $v = 2$. Now we have a much increased difference in generated voltage between the case of $v = 200$ and 2, namely, up to 260 mV (at $i = 4$ A). Reducing k_A by a further factor of 10^2 results in a difference in generated voltage between the $v = 200$ and 2 case of 270 mV at $i \sim 0.2$ A. In conclu-
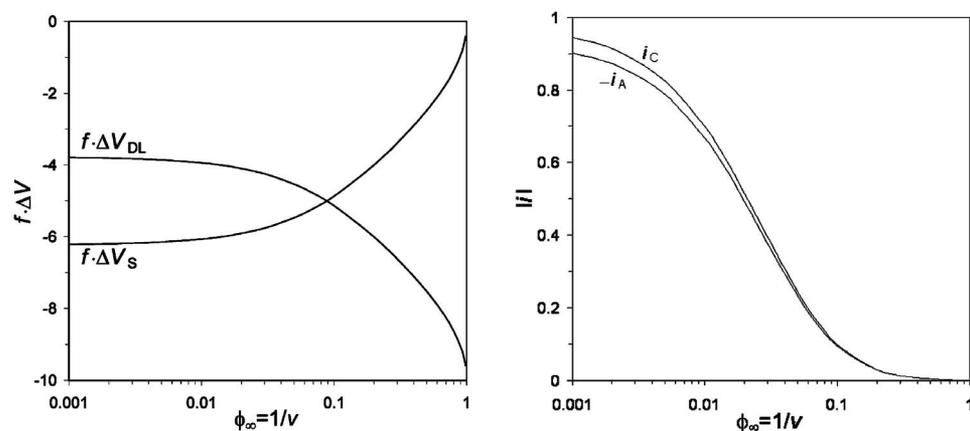

Figure 5. Influence of proton volume constraints on the structure of the polarization layer and the resulting electrochemical reaction rates ($\delta = 1$, $f\Delta V_T = -10$, $k_A = k_C = 1$ A/bar$^{1/2}$, $p_{H_2,j}$ and p^* as in Fig. 3).
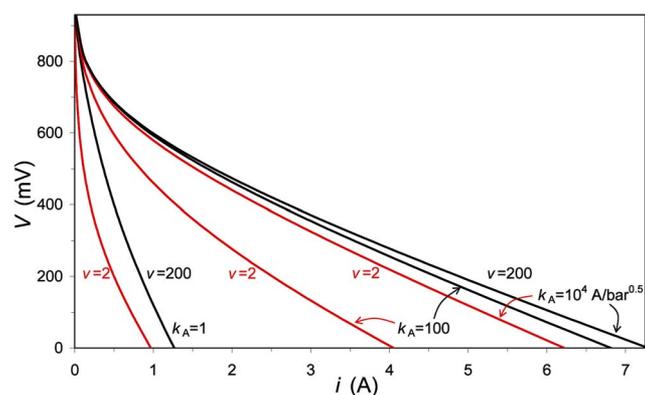
Figure 6. (Color online) Influence of proton volume constraints on the generated cell voltage V as function of current i ($\delta = 1$, $k_C = 10^4$ A/bar$^{1/2}$, $R_{elyt} = 68.9$ mΩ).

sion, although volume constraints do not have as large an impact in the concentration cell model as they do in a sub-calculation for a polarization layer with fixed ΔV_T, volume constraints can significantly influence predicted cell performance, reducing the generated voltage at a given current, compared to dilute-solution theory.

Conclusions

We have developed simple, general models for diffuse-charge effects in fuel cell membranes and applied them to the case of a steady-state concentration cell. This approach goes beyond the standard model, based on the BV equation for the electron charge transfer rate across a neutral membrane, while remaining analytically tractable and physically transparent. At equilibrium, we present an analytical expression for the proton charge in the polarization layer as a function of hydrogen pressure. In the Helmholtz limit of a very low polarization layer thickness relative to the Stern layer thickness, the state-of-the-art representation of the BV equation for a neutral membrane is recovered, but corrections due to nonzero diffuse charge can also be calculated. In the Helmholtz limit, as well as in the opposite GC limit, simple analytical expressions are obtained for generated voltage as function of current. For the first time in fuel cell modeling, to our knowledge, ion volume constraints are also included in the model via a modified PB equation for the polarization layer and a modified equation for the charge transfer rate. Compared to dilute-solution PB theory, the concentrated solution model predicts a substantially modified structure of the polarization layer and a reduction in the generated cell voltage due to an increased crowding of finite-sized ions.

Acknowledgments

References

1. J. O. Bockris and A. K. N. Reddy, *Modern Electrochemistry*, Plenum, New York (1970).
2. A. J. Bard and L. R. Faulkner, *Electrochemical Methods*, John Wiley & Sons, Hoboken, NJ (2001).
3. J. S. Newman, *Electrochemical Systems*, Prentice-Hall, Englewood Cliffs, NJ (1973).
4. R. O'Hayre, S.-W. Cha, W. Colella, and F. B. Prinz, *Fuel Cell Fundamentals*, John Wiley & Sons, Hoboken, NJ (2006).
5. W. G. Bessler, S. Gewies, and M. Vogler, *Electrochim. Acta*, **53**, 1782 (2007).
6. A. Frumkin, Z. *Phys. Chem. Abt. A*, **164**, 121 (1933).
7. R. Parsons, *Adv. Electrochem. Electrochem. Eng.*, **1**, 1 (1961).
8. B. B. Damaskin, V. A. Safonov, and N. V. Fedorovich, *J. Electroanal. Chem.*, **349**, 1 (1993).
9. A. Bonnefont, F. Argoul, and M. Z. Bazant, *J. Electroanal. Chem.*, **500**, 52 (2001).
10. A. A. Franco, P. Schott, C. Jallut, and B. Maschke, *Fuel Cells*, **7**, 99 (2007).
11. E. M. Itskovich, A. A. Kornyshev, and M. A. Vorotyntsev, *Phys. Status Solidi A*, **39**, 229 (1977).
12. A. A. Kornyshev and M. A. Vorotyntsev, *Electrochim. Acta*, **23**, 267 (1978).
13. A. A. Kornyshev and M. A. Vorotyntsev, *Electrochim. Acta*, **26**, 303 (1981).
14. M. Z. Bazant, K. T. Chu, and B. J. Bayly, *SIAM J. Appl. Math.*, **65**, 1463 (2005).
15. K. T. Chu and M. Z. Bazant, *SIAM J. Appl. Math.*, **65**, 1485 (2005).
16. A. A. Franco, P. Schott, C. Jallut, and B. Maschke, *J. Electrochem. Soc.*, **153**, A1053 (2006).
17. A. A. Franco and M. Gerard, *J. Electrochem. Soc.*, **155**, B367 (2008).
18. A. A. Franco, *ECS Trans.*, **6**(10), 1 (2007).
19. A. A. Franco and M. Tembely, *J. Electrochem. Soc.*, **154**, B712 (2007).
20. S. Chen and A. Kucernak, *J. Phys. Chem. B*, **108**, 13984 (2004).
21. M. R. Gennero de Chialvo and A. C. Chialvo, *Phys. Chem. Chem. Phys.*, **6**, 4009 (2004).
22. J. X. Wang, T. E. Springer, and R. R. Adzic, *J. Electrochem. Soc.*, **153**, A1732 (2006).
23. C. D. Taylor, S. A. Wasileski, J.-S. Filhol, and M. Neurock, *Phys. Rev. B*, **73**, 165402 (2006).
24. M. Ni, M. K. H. Leung, and D. Y. C. Leung, *Fuel Cells*, **7**, 269 (2007).
25. K. C. Neyerlin, W. Gu, J. Jorne, and H. A. Gasteiger, *J. Electrochem. Soc.*, **154**, B631 (2007).
26. F. Jaouen, G. Lindbergh, and G. Sundholm, *J. Electrochem. Soc.*, **149**, A437 (2002).
27. M. Eikerling, *J. Electrochem. Soc.*, **153**, E58 (2006).
28. M. S. Kilic, M. Z. Bazant, and A. Ajdari, *Phys. Rev. E*, **75**, 021502 (2007).
29. P. M. Biesheuvel and M. van Soestbergen, *J. Colloid Interface Sci.*, **316**, 490 (2007).
30. M. Z. Bazant, K. Thornton, and A. Ajdari, *Phys. Rev. E*, **70**, 021506 (2004).
31. A. A. Kornyshev, *J. Phys. Chem. B*, **111**, 5545 (2007).
32. J. J. Bikerman, *Philos. Mag.*, **33**, 384 (1942).
33. V. Freise, Z. *Elektrochem.*, **56**, 822 (1952).
34. D. Lacoste, G. I. Menon, M. Z. Bazant, and J. F. Joanny, *Eur. Phys. J. E*, Accepted.
35. M. Z. Bazant, D. Lacoste, and K. Sekimoto, To be published.
36. G. Singh, G. Ceder, and M. Z. Bazant, *Electrochim. Acta*, **53**, 7599 (2008).
37. C. Y. Wang, *Chem. Rev. (Washington, D.C.)*, **104**, 4727 (2004).
38. L. Pisani and G. Murgia, *J. Electrochem. Soc.*, **154**, B793 (2007).
39. W. G. Bessler, J. Warnatz, and D. G. Goodwin, *Solid State Ionics*, **177**, 3371 (2007).
40. H. Ju and C.-Y. Wang, *J. Electrochem. Soc.*, **151**, A1954 (2004).
41. R. F. Mann, J. C. Amphlett, M. A. I. Hooper, H. M. Jensen, B. A. Peppley, and P. R. Roberge, *J. Power Sources*, **86**, 173 (2000).
42. D. M. Bernardi and M. W. Verbrugge, *J. Electrochem. Soc.*, **139**, 2477 (1992).
43. G. Murgia, L. Pisani, M. Valentini, and B. D'Aguanno, *J. Electrochem. Soc.*, **149**, A31 (2002).
44. S. Kakaç, A. Pramauanjaroenkij, and X. Y. Zhou, *Int. J. Hydrogen Energy*, **32**, 761 (2007).